THE DLR FIREBIRD MISSION - A TECHNOLOGICAL EXPERIMENT FOR OPERATIONAL WILD FIRE MONITORING

Olaf Frauenberger[1], Erik Borg[1], Winfried Halle[2], Eckehard Lorenz[2], Jens Richter[1], Thomas Terzibaschian[2]

[1] *German Aerospace Center, German Remote Sensing Data Center. Neustrelitz*
[2] *German Aerospace Center (DLR), Institute of Optical Sensor Systems, Berlin*

Introduction

The FireBIRD mission is a constellation of two small satellites designed and developed by DLR Optical Systems in Berlin-Adlershof with contributions from other Institutes of DLR. The first satellite TET-1 was launched in 2012 from Baikonur, the second satellite BIROS was launched in 2016 from Satish Dhawan Space Centre (India). The mission is inherited from the BIRD satellite operated from 2001 to 2004 [1]. Both satellites host a number of technological experiments, of which the main payload common to both satellites is the multispectral camera system (MSC) with spectral channels in the visible (VIS), medium infrared (MWIR) and thermal or long wave infrared (LWIR) designed to detect and observe high temperature events.

Thermal remote sensing (RS) is useful to monitor low-temperature events and their spatio-temporal dynamic for deriving environmental information, or to detect man-made or environmental high-temperature events, their expansion and distribution. High temperature applications are e.g. the identification and monitoring of artificial and natural hotspots like wildfires [2], volcanoes [3], or Gas Flaring. In the low-temperature range RS is used to monitor, e.g. the temperature of sea and lake surfaces [4], and urban structures.

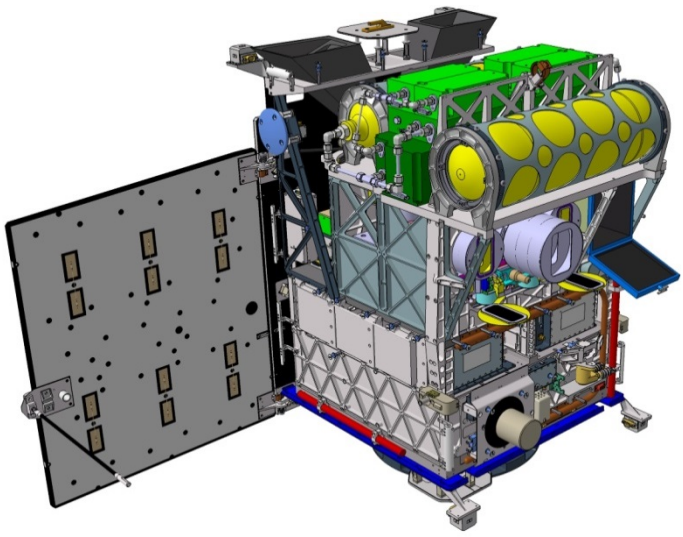

Fig. 1. BIROS satellite

Platform for Technological Experiments

Both satellites, TET-1 and BIROS, have a similar structure with a payload compartment hosting a number of technological experiments. In case of TET-1 the technological experiments where conducted by ASTRIUM focusing on monitoring the functionality and performance of new devices as such. It was successfully demonstrated, that a small satellite can be used as a low coast approach for testing new technologies before they will be applied on larger experiments or become mission critical. For BIROS a next step has been done by the design of new methods in space operation for which also new devices have been developed [1].

- AVANTI - Autonomous orbit maneuvers by optical navigation through star cameras and thruster control and On-board Mission planning
- Picosat - used as target of proximity operations with AVANTI
- Cold Gas Propulsion System used for proximity operations with AVANTI
- ORBCOMM modem planned for messages with extracted fire product parameter
- OSIRIS - Optical Uplinks and Downlinks with Laser-Beams
- High Torque - New actuators for high agility satellite maneuvers

At the current state the satellite is still in commissioning phase. The experiment AVANTI has been performed successfully with the launch of Picosat and the Cold Gas Propulsion System involved [5].

Theoretical Background High Temperature Events Observation

Optical and thermal remote sensing are based on the principle that warm bodies emit electromagnetic radiation depending on their temperature as it is described by Planck's law for an ideal black body:

$$L_\lambda(\lambda, T) = \frac{2hc^2}{\lambda^5\left(\exp\left(\frac{hc}{\lambda kT}\right)-1\right)}, \left[\frac{W}{m^2 \mu m \cdot sr}\right], \quad (1)$$

Equation 1 formulates the relation between the spectral radiance of a perfect emitter $L_{BlackBody}$ and the kinetic temperature T [K] and wavelength λ [µm] with the Planck's constant h [$6.62607 \cdot 10^{-34}$ Ws^2], the Boltzmann's constant k [$1.380648 \cdot 10^{-23}$ $Ws\ K^{-1}$], and the speed of light in vacuum c (299,792,458 ms^{-1}). A direct relationship between the maximum of radiation and the wavelength is expressed in Wien's displacement law:

$$\lambda_{max}(T) = T^{-1} 2898\ \mu m\ K \quad (2)$$

The relationship between reflected and emitted radiation is expressed by Kirchhoff law:

$$\varepsilon + \tau + \varrho = 1 \quad (3)$$

where ε is emissivity, τ is transmission and ρ is the reflection of an object. Perfect emitters with $\varepsilon = 1$ are called black bodies, while a value of $\varepsilon < 1$ indicates a so called grey body.

Solar irradiance, which can be approximated by a black body, having a surface temperature of 6000 K, has its peak intensity at a wavelength of 0.480µm. The radiation emitted by the earth surface can be approximated by a gray body, with an assumed average temperature of 300 K having a maximum intensity at 9.7 µm, while the maximum intensity for a wild fire with temperatures ranging from 600 to 1500 and a typical value of at 800 K [2] is located at a wavelength of 3.6 µm. Since the atmosphere contains also absorbers water, trace gases, especially O_3 andCO_2, and aerosols, the spectral ranges of the sensor need to be adjusted to the atmospheric windows close to the selected wavelength (Fig. 2).

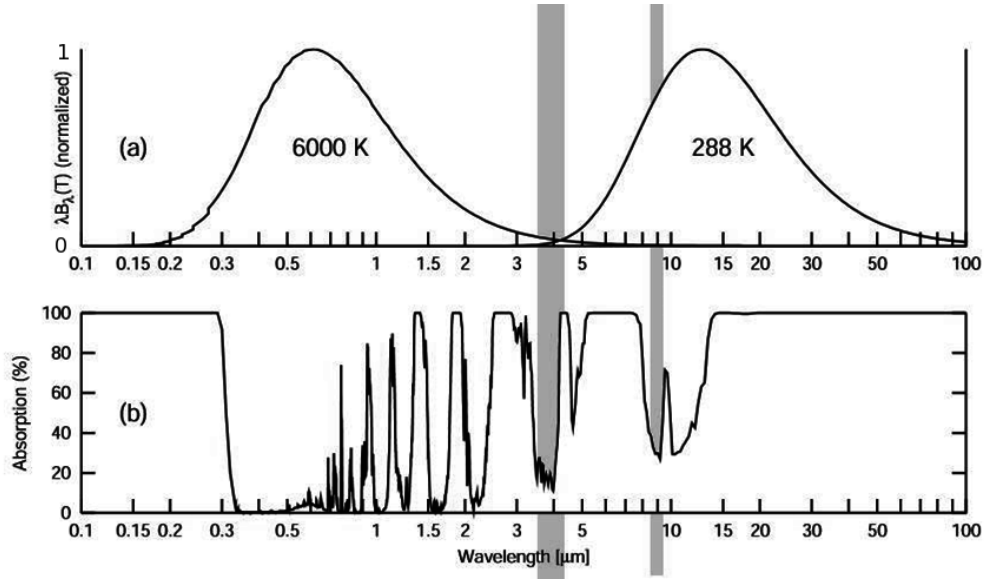

Fig. 2 Top: Solar irradiation (6000K) normalized at earth distance and sea surface temperature (288K), Bottom: Atmospheric transmission, marked spectral windows in MWIR (3.8 µm) and LWIR spectral window (8.6 µm) adopted by Rodgers.

In typical wildfires the emitted radiance L_g^e at ground comprises two parts, the fire emitted radiance L_F^e with the active fire area A_F, covering only a small fraction of a ground pixel, and the radiance flux $L_{bg}^e(\lambda, T_{bg})$ originating from the background (eq 4) using a model based emission coefficient ε_{bg}.

$$L_G^e(\lambda) = A_F \varepsilon_F(\lambda) L_F^e(\lambda, T_F) + [1 - A_F]\varepsilon_{bg}(\lambda) L_{bg}^e(\lambda, T_{bg}), \text{ with } A_F \ll 1 \quad (4)$$

For estimation of the background contribution a Long Wave Infrared (LWIR) channel can be used. In space borne observations contributes also the atmosphere to the signal at sensor $L_{as}(\lambda)$:

$$L_{as}(\lambda) = \varepsilon_{atm}(\lambda) L_{atm}^e(\lambda) + \varrho_{atm}(\lambda) L_{atm}^s + \tau_{atm}(\lambda)\{\varepsilon_g(\lambda) L_g^e(\lambda) + [1 - \varepsilon_g(\lambda)] L_g^s\} \quad (5)$$

The spectral transmission coefficients $\tau_{atm}(\lambda)$ of the atmosphere are based on MODTRAN estimations. The emitted radiance of the atmosphere $L_{atm}^e(\lambda, T_{atm})$ can be neglected. In day light conditions we have to consider also reflected solar radiance

$L^s_{atm}(\lambda)$. In a clear atmosphere and for canopy layers the reflection coefficients ϱ_{atm} and $\varrho_g = 1 - \varepsilon_g$ are small, and can be therefore neglected. However in the presence of clouds or direct reflections on high reflective surfaces, e. g. water, scattered sun light can cause strong disturbances leading to false alerts. Therefore, for day time observations a third channel in the visible spectral is required, providing information on reflected sun light. But also for deriving additional information on the canopy layer or for detection of burned areas visible spectral channels are useful.

Based on these considerations the multispectral camera system for the FireBIRD mission has been designed. Its technical parameters are listed in Table 1.

Table 1

Technical characteristics of FireBIRD multispectral camera platform (MSC)

	3 line-VIS Camera (3 lines 6° separated)	2 Infrared- Cameras (staggered lines)
Wave length	Green: 460 - 560 nm Red: 565 - 725 nm NIR: 790 - 930 nm	MWIR: 3,4 - 4,2 µm LWIR: 8,5-9,3 µm
Detector	CCD- Array	CdHgTe Arrays
Detector cooling	Passive, 20°C	Stirling, 100 - 80 K
Pixel size	7 µm x 7 µm	30 µm x 30 µm
Number of Pixel	3 x 5164 (1250)	2 x 512 staggered
Quantization	14 bit	14 bit
Ground resolution	42 m [1)]	356 m [1)]
Ground sampling distance	42 m [1)](160 m binned)	178 m [1)]
Swath width	211 km [1)]	178 km [1)]
Data rate	max 44 MBit/s	0,35 MBit/s
Accuracy	100m on ground	100m on ground

[1)] At an initial altitude of 510 km

Although the instantaneous field of view (IFOV) for the thermal cameras is ≈340m, the ground sampling distance (GSD) is ≈170 m. Since the IR detectors are arranged in pairs of staggered lines, hence one pair of adjacent located lines, where the second line is shifted by half a pixel size, an overlap of two ground pixels across track exists. Along track the image is sampled within an interval of ≈ 20ms while the flight duration of a full thermal pixel size is ≈ 40ms causing an overlap in flight direction. As a result, a point source activates 4 pixels in the image (Fig. 7).

Within the sampling interval of 20 ms it is possible to make a second exposure with a shorter integration time, e. g. 0.5 ms instead of 4 ms, to avoid saturation, and therefore extend the dynamic range of the IR-sensor.

Case Studies of Thermal Remote Sensing

Beside the observation of high temperature events normal temperature applications are important as well. Areas of interest are observations with moderate geometric resolution, such as sea surface temperatures, monitoring of medium sized inland water bodies or heat islands in urban areas.

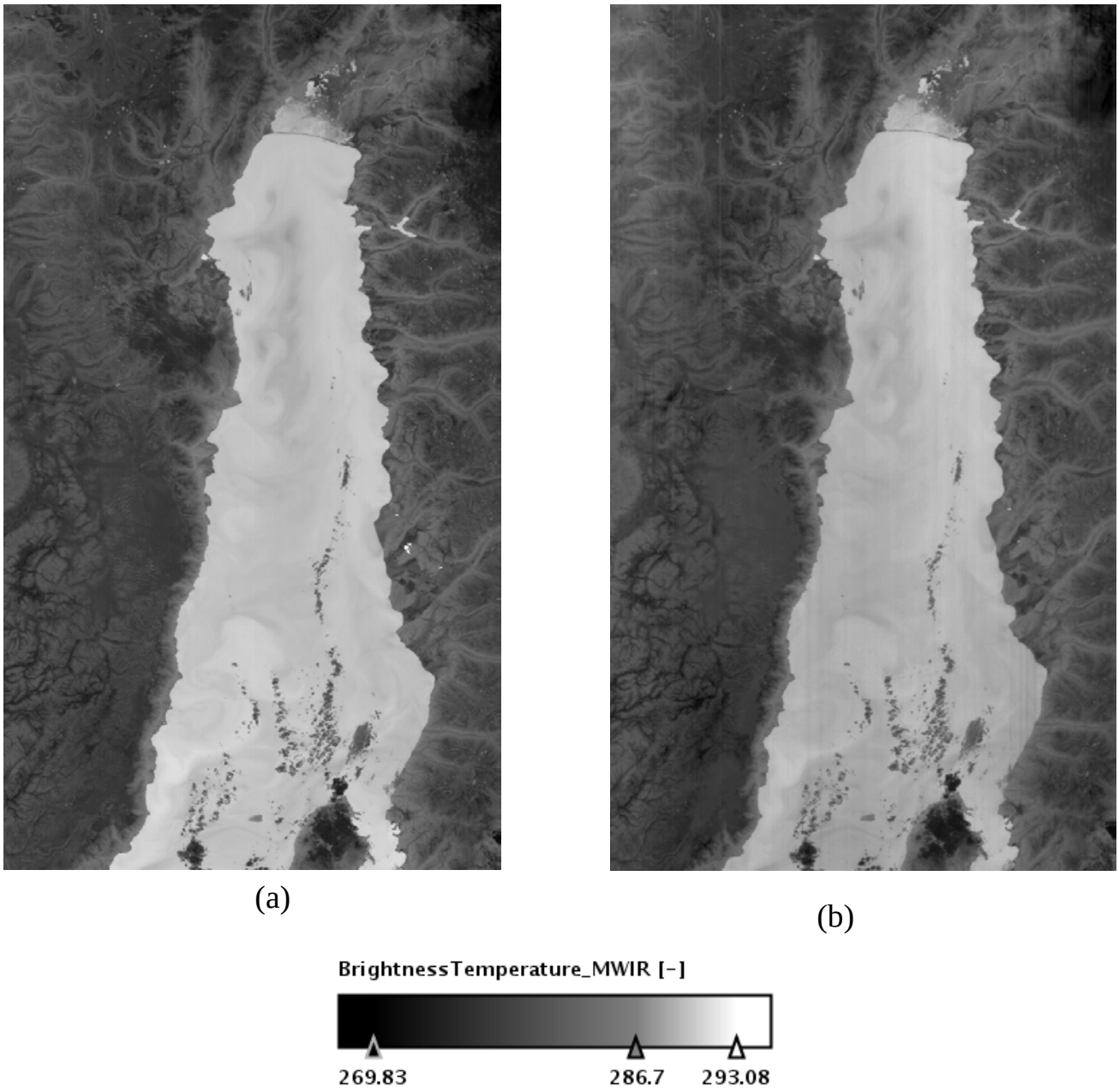

Fig. 3 Lake surface temperature of lake Baikal 1from 03.09.2016 19:00 UTC with (a) MWIR channel at 3.8 µm, and (b) LWIR channel at 8.9µm in [K]

A preferred target for thermal camera observations are lakes, since the offer a more or less homogeneous area, and especially the emission coefficient for water is with $\varepsilon = 0.977$ very close to 1 and shows only little variations within the medium and thermal infrared spectral range. Therefore water bodies represent a good

approximation of a black body in thermal remote sensing and can be used for validation purposes. However the variability of atmospheric transmission needs to be considered as well. In case of the infrared spectral channels of the MSC, the main influence is given by atmospheric H_2O.

The temperatures derived from both IR channels are shown in Fig. 3 in comparison. A fixed atmospheric correction has been applied to those images, local variable differences are visible. Based on two independent channels a simplified model with two sources unknown parameter can be used, where the first is the ground temperature and the second is atmospheric H_2O. Such a model is used e. g. optimal estimation algorithm [7] or in the split window method [8].

A subsection of the scene shown in Fig. 3containing an active forest or peat fire at the East of Lake Baikal is shown Fig. 4.

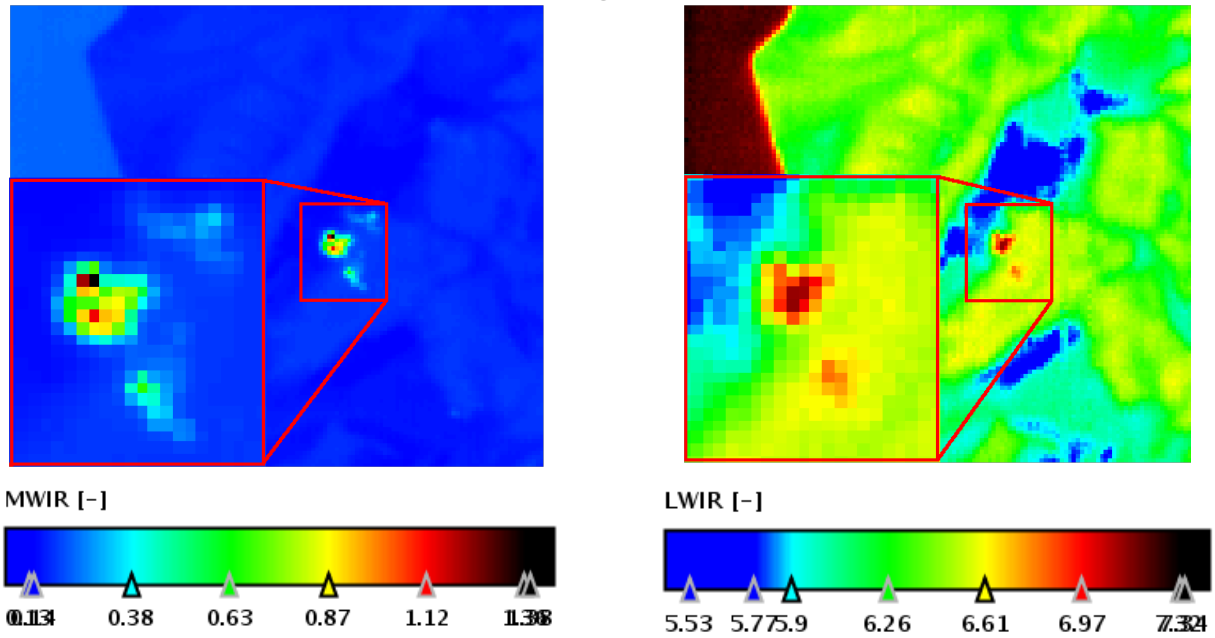

Fig. 4 Spectral radiance images of MWIR and LWIR showing a forest fire, detected east of lake Baikal scaled in [W / (m^2·µm·sr)] with the lake at the top left, while the dark cool area in the middle represent clouds

Table 2

Detected fire parameter in Scene from 03.09.2016 19:00 UTC

Cluster Size, Pixel	Lat, degree	Lon, degree	FRP, MW	T_{min}, K	T, K	T_{max}, K	A_{min}, m^2	A, m^2	A_{max}, m^2
40	54.54	109.60	33	460	502	586	3098	9189	18230
8	54.52	109.60	2,7	500	531	577	340	603	935

While in the thermal channel (LWIR) the signal level raised by the fire shows in relation to the absolute value only a little difference to the surrounding area and is equal to the surface signal of the lake, the signal observed in the MWIR channel

caused the fire is a magnitude higher compared to the surrounding. Due to the relative high geometrical resolution, it is also possible to separate active burning areas. In the image shown, two of the detected hot clusters have been detected and flagged as reliable. The estimated parameters are listed in Table 2.

For fire detection and parameter estimation the Dozier algorithm is used adapted by B. Zhukov for the BIRD satellite [6]. Essential for the reliability and avoidance of false alerts is the screening of the background for clouds, sun glint in a visible channel and for thermal anomalies in the LWIR channel. For a precise quantitative estimation the background signal needs to be correctly selected and estimated, since the size of the active fire covers only a fraction of the activated pixels within the fire cluster (Eq. 4).

Other sources of thermal radiation within the field of environmental monitoring are gas flares on oil wells. They contribute significantly to greenhouse gas emission and to local air-pollution.

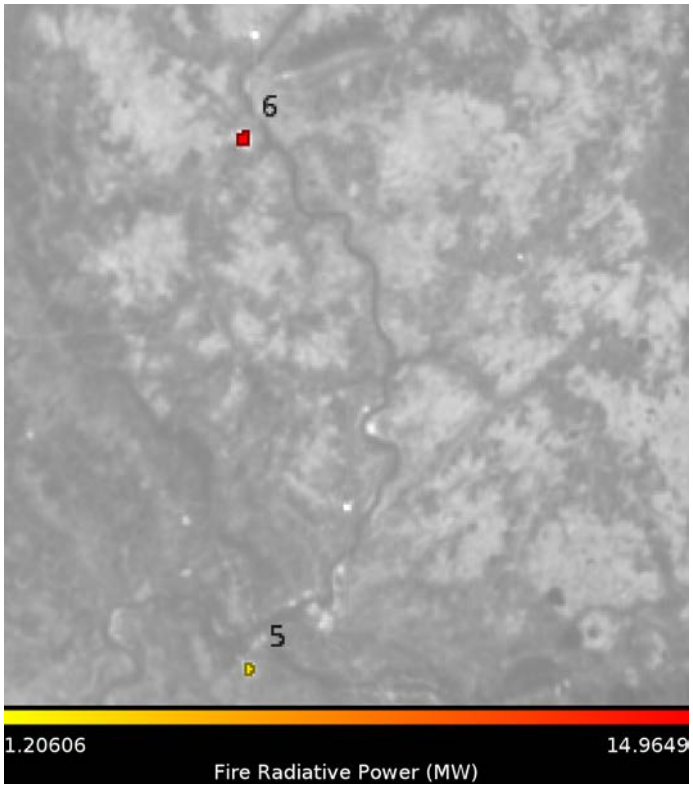

Fig. 5 Burning gas flares at oil wells in Usinsk / Komi at 23.07.2016 08:48 UTC. Detected flares are marked and coded with color according to intensity. Some flares are not detected since they are below the detection threshold

Gas flares represent a local fixed point source, however with fluctuations with respect to intensity. Since the detection algorithm is adjusted to fire, weak flares are below the detection threshold although they are visible in the image Fig. 5. For reliable detection, separate filters are needed, adjusted to local conditions in order to avoid false alerts.

Compared to gas flares volcanoes emit much higher radiation as shown in Fig. 6. For observation of the active section of the Bardarbunga eruption (shaded area),

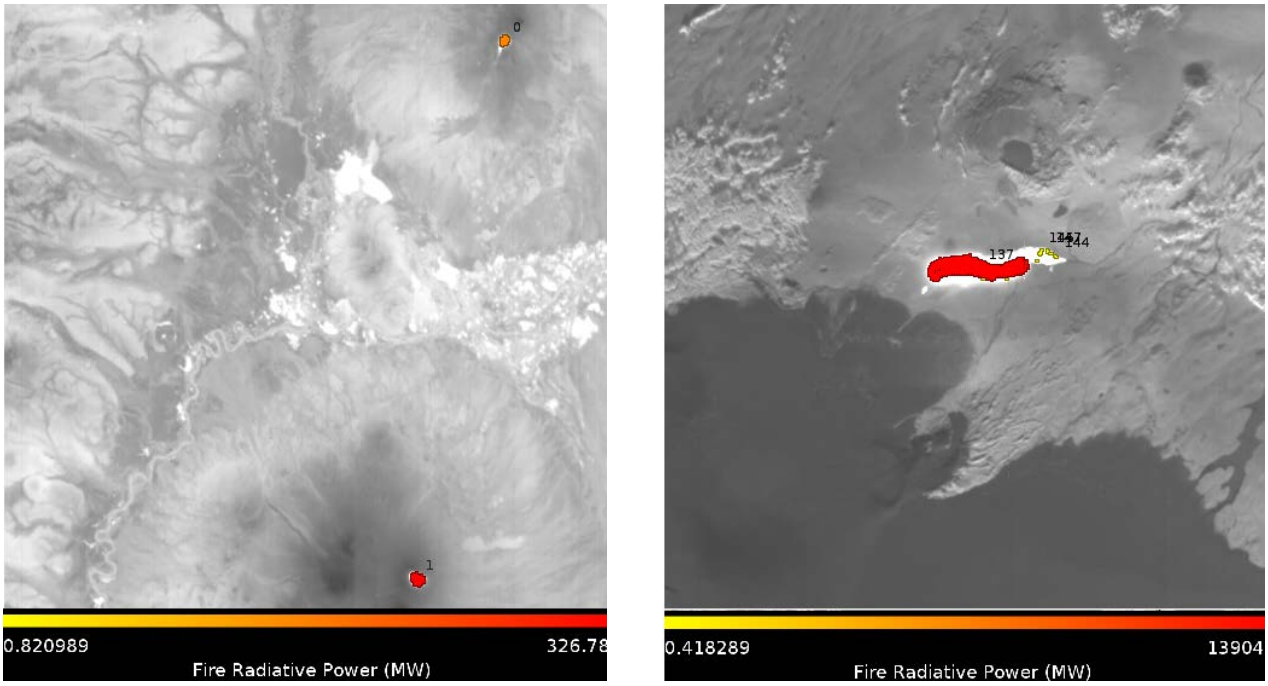

(a) (b)

Fig. 6 Active volcanoes Ključevskaja group (Kamchatka) 23.June 2016 (a) and Bardarbunga Island

saturated pixels have been replaced with data from the second shorter signal acquisition, while the same scene is covered with ice in the lower part.

Table 3

Estimated parameter of volcanoes in Fig. 6 (0 - vlk. Šiveluč, 1 - vlk. Ključevskaja Sopka, 137- Bardarbunga)

	Cluster Size, Pixel	FRP, MW	T_{min}, K	T, K	T_{max}, K	A_{min}, m^2	A, m^2	A_{max}, m^2
0	46	83	474	486	500	39820	49660	60363
1	85	84	755	766	778	15467	16710	17995
137	1047	13905	570	577	584	2042415	2212299	2386176

Comparing the estimated parameter in Table 3, the relationship between the hot cluster size in the image and the estimated size of the hot area shows the influence of the temperature.

Validation of Fire Parameter

In order to proof whether estimated parameter obtained from the satellite observations are correct, a validation campaign had been performed. For this a test fire design has been made and deployed at the calibration side DEMMIN® in north-

east Germany [9]. Within this area a network of meteorological stations provides environmental information. The test burn has been performed on 17. August 2013.

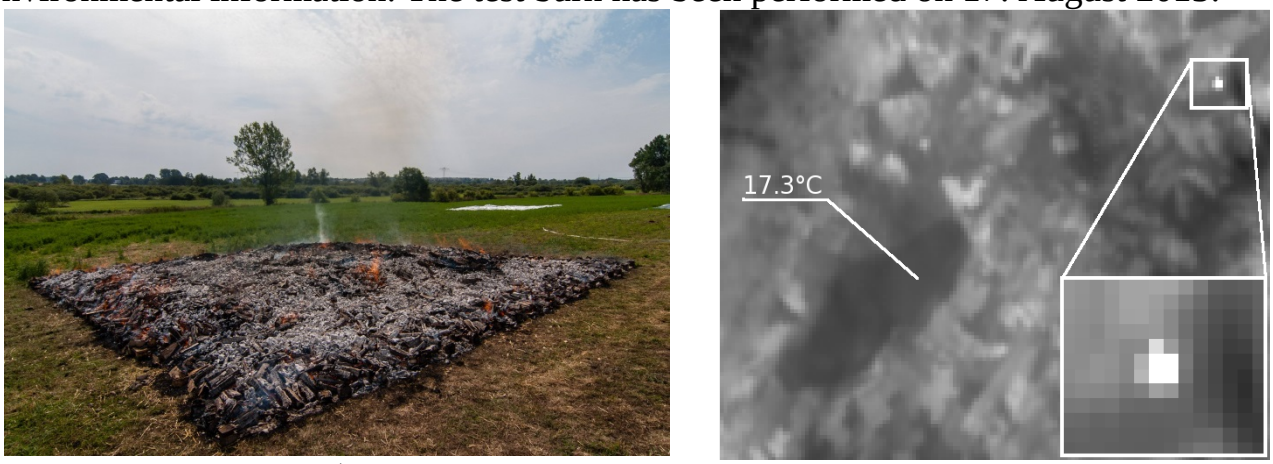

a) b)

Fig. 7 a) Test Fire at test site DEMMIN with size of 12x13 m^2 and 940K [Borg]
b) Estimated lake surface temperature and fire plot seen in the MWIR channel

The aim of the test was to create a fire at the low detection threshold of the sensor with a well specified dimension and a homogeneous surface temperature to be kept constant within a specific time window.

Table 4

Comparison of Remote Sensing data with ground measurements at the fire experiment

	FRP, MW	T_{min}, K	T, K	T_{max}, K	A_{min}, m^2	A, m^2	A_{max}, m^2
In-situ	1,36	300	940	1150	-	143	-
TET-1	2,27	488,3	720	1500	8,9	148,3	1821

The estimated FRP, an abstract parameter to describe the fire with respect to biomass consumed, was 1.3 times larger than calculated [10]. This and also other campaigns, where helicopter measurements have been compared with TET-1 derived parameter, show an error margin between 20 to 60percent. Most critical is the correct estimation of the background radiance, due to fact that the active fire covers only 0.13% of the pixel area.

Ground segment and data processing

The ground segment consists of mission planning and monitoring performed by the German Space Operation center in Oberpfaffenhofen and Ground Station Network of DLR with National Ground Segment in Neustrelitz as main station. From Neustrelitz the uplink for tele commands takes part and also the majority of downlink activities. Downlink data also from other DLR stations in Inuvik (Canada) and O-Higgins (Antarctic Peninsula) is collected, separated according to their origin at the spacecraft and shortly after completion distributed via FTP.

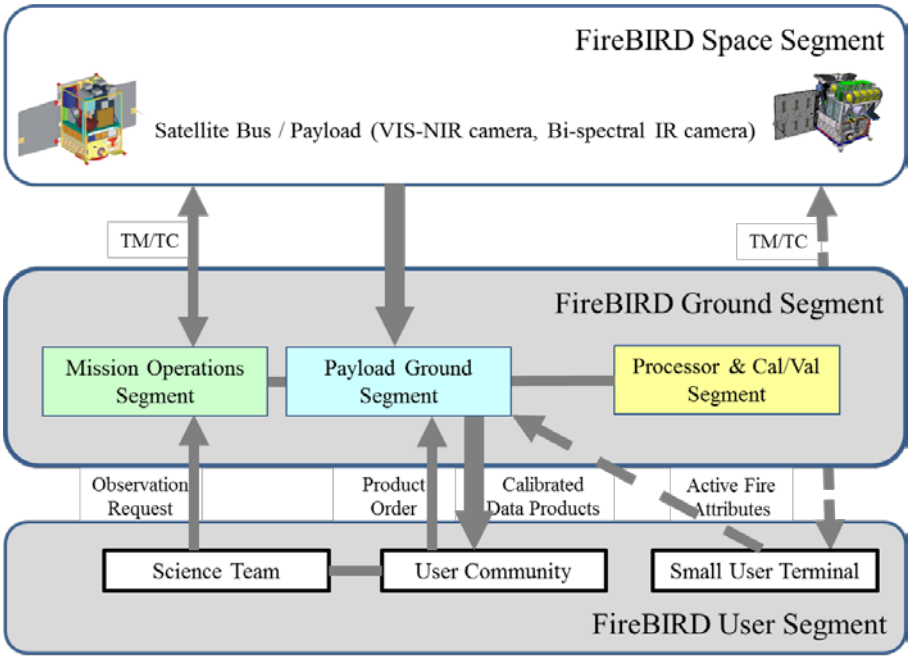

Fig. 8 Structure of ground segment (J. Richter)

The data stream of the MSC is processed automatically in near real time in two processing steps, first to so-called Level 1B images containing spectral radiances with geolocation annotation. The second processing step consists of thematic Level 2 fire processing. It consists of a co-registered image of the MWIR, LWIR and Red channels at the grid of the MWIR channel, a table with detected hot areas including events marked as uncertain, a fire mask and a quick look. Products are provided as raster images in two formats, Envi-format combined with an XML file and csv-table, and as HDF5-EOS format. The products are delivered to an FTP server where users can retrieve the data. Level 0 raw data are archived together with meta-information retrieved during Level 1B and Level 2 processing. The camera platform operates in discontinuous mode, which means an observation for a given location of interest and time period needs to be scheduled 3 to 1 days in advance. The typical size of an observed area is approximately 400x200 km. All products are freely available on the DLR Earth Observation on the WEB (EOWEB) site (https://geoservice.dlr.de/egp/) for self-registered users. The tool owns search capabilities for location and time frames and provides meta and statistical information on the selected products, e. g. the number of detected fires. For registered science users it is possible to place orders for distinct areas within certain time periods.

Conclusion

The mission demonstrates that small satellites can be used to support new technological and scientific experiments, while reducing costs and risks compared to big satellite missions. Even with the delay of the launch of the second satellite BIROS it was possible to expand the operational life-time of the TET-1 satellite. Experiences gained with BIRD have been used to improve the system.

Since the resources of a small satellite are limited, about 5 to 7 acquisitions per day are performed. Main restrictions to data acquisition results from energy budget, capacities of the on-board memory, and downlink capacities. Even with further technical improvements increasing the budgets, an increasing data rate provided by better sensors, limits will remain. Therefore it is necessary to reduce the amount of data by pre-selection of high temperature events and /or by de-selection of image parts obscured by clouds. Other experiments on BIROS deal with these questions, OSIRIS to increase the downlink capacity via laser and advanced data processing on-board of the satellite for thematic data reduction.

L i t e r a t u r e

1. *Halle, W., Terzibaschian, T., Bärwald, W., Schultz, C.* Results of the DLR FireBird Constellation. // Small Satellites for Earth Observation 11th Symposium of the IAA. Berlin 2017. IAA-B11-0201
2. *Wooster M.J., Zhukov B., Oertel D.* Fire radiative energy for quantitative study of biomass burning: derivation from the BIRD experimental satellite and comparison to MODIS fire products. // Remote Sensing of Environment 86 (2003) 83 - 107
3. *Ramsey, M.S. Harris, A.J.L.* Volcanology 2020: How will thermal remote sensing of vol-canic surface activity evolve over the next decade? // Journal of Volcanology and Geothermal Research 249, 217-233 (2013)
4. *Wloczyk, C., Richter, R., Borg, E., Neubert, W.* Sea and lake surface temperature retrieval from Landsat thermal data in Northern Germany. // International Journal of Remote Sensing 27, 2489-2502 (2006)
5. *Gaias G., Ardaens J.S., Schultz, C.* The AVANTI Experiment: Flight Results. // 10th International ESA Conference on Guidance, Navigation & Control Systems, 29 May - 02 Jun 2017, Salzburg
6. *Zhukov, B., Lorenz, E., Oertel, D., Wooster, M., Roberts, G.* Experience of detection and quantitative characterization of fires during the experimental small satellite mission BIRD. DLR-Forschungsbericht 2005, 04.
7. *Mettig, N.,* Sensitivitätsstudie zur Bestimmung der Meeresoberflächentemperatur aus Messungen des Satelliten TET-1. Masterarbeit DLR, Freie Universität Berlin. Berlin. 29. June 2016.
8. *Hulley, G.C., Hook, S.J., Baldridge, A.M.,* Generating consistent land surface temperature and emissivity products between ASTER and MODIS data for Earth science research. // IEEE Trans. Geosci. Remote Sens. 2011, 49, (4), 1304–1315
9. *Gerighausen, H., et. al.* DEMMIN—A test site for the validation of Remote Sensing data products. // In Proc. on AGRISAR and EAGLE Campaigns Final Workshop, ESA/ESTEC, October 15–16, 2007, Noordwijk, Netherland. P.1–9, 2007.
10. *Borg, Erik et. al.* High Temperature Fire Experiment for TET and LANDSAT 8 in Test Site DEMMIN (Germany). // 17th International Conference on Computational Science and Applications (ISI) - Theoretical Computer Science and General Issues (Series Volume: 10406). 2017, Trieste